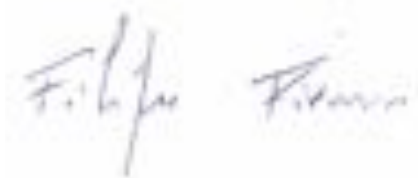


Numerical modelling of a structural adhesive used for bonding hybrid steel-glass beams

COST Action TU1403
“Adaptive Facades Network”

Short Term Scientific Mission
COST-STSM-ECOST-STSM-TU1403-301115-068846
University of Trieste
30/11/2015 to 05/12/2015

A handwritten signature in dark ink, appearing to read 'Filipe Firmo', is centered on the page.

Visitor: Mr. Filipe Firmo, University of Coimbra (Portugal)

A handwritten signature in blue ink, appearing to read 'Chiara Bedon', is centered on the page.

Host: Dr. Chiara Bedon, University of Trieste (Italy)

1. Introduction / Objectives

In the last few years, technological developments of the glass industry have increased the use of glass with load bearing purposes. Glass brittle behaviour and its low tensile strength is being overcome by different approaches: the first and the most common one is making use of the tempering and lamination process by introducing high performance interlayers in laminated glass sheets to improve the structural behaviour of glass; the most recent is the development of adhesive connections to achieve an efficient composite behaviour between glass and the supporting elements or to combine glass with ductile materials in order to achieve an extra level of structural redundancy. The current work is within the framework of the latter approach.

In contemporary Architecture it is possible to notice a wide use of structural glass in façades where glass panels and fins interact with steel substructures, metal frameworks and other structural components through adhesive joints and mechanical connectors. The adhesive connections are gaining popularity because of their assembling potential, since an efficient composite behaviour between glass and the supporting elements may be achieved since it ensures a more uniform load transfer, unlike the bolted connections that weaken the glass near the boltholes. So, as expected, the load bearing characteristics of the façade significantly depend on the composite behaviour of the system, and subsequently, on the adhesive performance. Thus, it is of the utmost important to be able to accurately characterize it. Nevertheless, this task is not so straightforward for two main reasons: on one hand, the available commercial information about the behaviour of high performance adhesives for structural applications is not as complete as needed, especially if a nonlinear analysis is envisaged; on the other hand, the numerical modelling of non-rigid structural adhesives that are rubber-like materials, require the implementation of hyperelastic rheological models. The choice of the appropriate model in a specific problem requires the necessary calibration of its corresponding parameters, which should ideally be established from dedicated and tailored experimental tests.

The main objective of the proposed STSM addresses this topic and consists in the characterization of the behaviour of structural adhesives of common use and the selection of the appropriate model to deal with it in the *Abaqus* software. This STSM goal is in line with the COST Action TU1403 objectives, and specifically with the activities of its sub-group “Structural Glass”.

It is intended to develop a Finite Element model in order to simulate the mechanical behaviour of the adopted polyurethane, under uniaxial tension and shear. Specific small-scale experiments have been performed on adhesive specimens under uniaxial tension and shear independently at the laboratories of the University of Coimbra before the Short Term Scientific Mission [12]. Their results will be used for choosing the most appropriate hyperelastic model and for establishing their corresponding parameters.

2. State of the art – Adhesives

Nowadays, there are many adhesives produced by different manufacturers, which can be potentially used for steel - glass connections. Most often used adhesives can be divided according to their modulus of elasticity and shear modulus into flexible-elastic (i.e. silicones, modified silicones and polyurethanes) and rigid (i.e. epoxy resin, acrylates) [4].

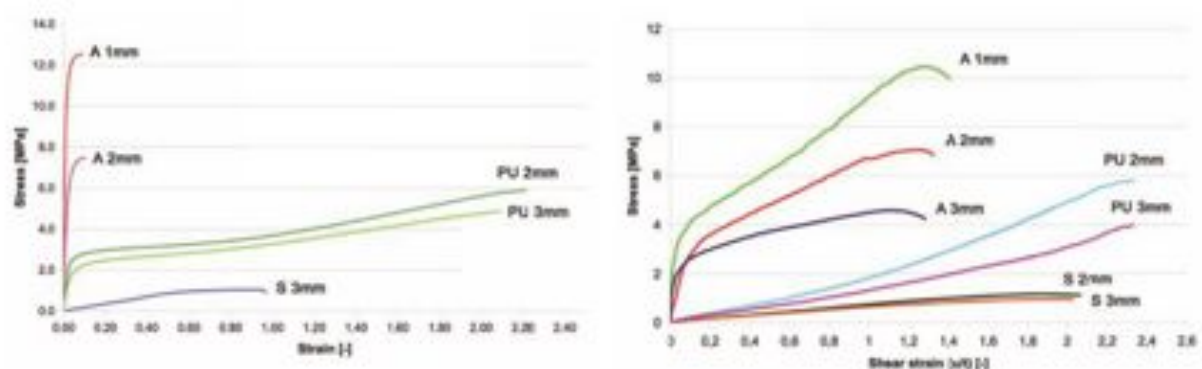


Figure 1 – Comparison of different adhesive types: S-silicone; PU – polyurethane; A-Acrylate [4]

Adhesive Type	General Properties
Silicones	Low strength and stiffness; High durability and resistance against moisture and UV-radiation; Hyperelastic material behaviour;
Polyurethanes	Medium strength and stiffness; Low resistance against UV-radiation; Hyperelastic material behaviour;
Acrylates	Generally high shear strength and small optimal thickness; Generally low resistance against moisture; Visco-plastic material behaviour;
Epoxies	High strength and stiffness but brittle; Small optimal thickness; Linear elastic material behaviour;

Table 1 – Different adhesive types and general properties (adapted from [16])

The selection of the most suitable adhesive is not straightforward, in the sense that the bonded joint must be rigid enough to provide an optimal structural interaction between the two materials for maximizing stiffness and resistance, but, on the other hand, it has to be flexible enough to redistribute the stress peaks in critical points and to mitigate the effects of different temperature elongation of steel and glass. Besides structural aspects, other factors have to be taken in account when selecting an adhesive, like the resistance to temperature, UV or even the colour. Finally, the thickness of the adhesive is also

conditioned by the geometrical imperfections of the surfaces to be bonded since these must be completely filled so that no voids are created.

In the scope of the INNOGLAST project [4], after the selection of some adhesives, in order to estimate some mechanical properties like the elastic modulus and the Poisson's ratio, uniaxial tension tests were performed in small-scale test specimens. The obtained stress-strain curves were not enough to characterize the adhesive due to the fact that, in the majority of the applications, the adhesive layer is subjected to shear. In order to have a complete knowledge of the adhesive behaviour, new tests were performed. The Innoglast final report made reference to four different test setups, where only two of them are standardized, see Table 2.



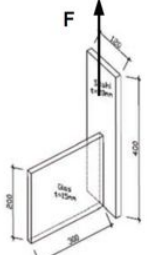
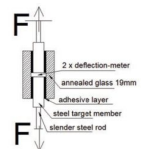
Single lap shear test (EN 1465 e EN 14869-2)	
Block shear test (EN ISO 13445)	
Push out shear test	
Steel-glass shear connection test	

Table 2 - Tests performed during the Innoglast project to characterize the shear behaviour of the adhesives [7];

Finite Element Analysis is widely used in the design of structures and sub-components. Suitable material models and accurate material test data are required to achieve accurate predictions of the adhesive behaviour. The majority of the adhesives cannot be accurately modelled using conventional elastic-plastic material models since they can develop very large strains under small stress states. These materials need more complex rheological models, like hyperelastic models. In order to accurately model hyperelastic materials under multi-axial states of stress, test data are required under conditions of plane stress (uniaxial tension), plane strain (planar tension) and equi-biaxial stress (equibiaxial tension) [1,3,17].

3. Case study - Hybrid steel-glass beams

The novel concept of hybrid steel-glass beams consists in using an adhesive bonding to assemble steel flanges to a glass web in order to increase the load carrying capacity, lateral stability, ductility and to achieve redundancy. The polyurethane Sikaforce 7710 L100 + 7010 was the selected adhesive to make the adhesive bond. This subject is currently being studied at University of Coimbra. The adhesive will act as a semi-rigid connector between steel and glass so, in terms of analytical or numerical modelling, it is essential an accurate simulation of its behaviour.

4. Experimental tests

4.1. Uniaxial tension test

The test specimens were prepared and cut in a dumbbell shaped form according to the ASTM D883 standard [7]. A 3.8mm/min rate was considered until fracture occurred. The geometry of the specimen is shown in the following figure. More details about the experimental setup and the test procedure can be found in [7]. Figure 3 illustrates the nonlinear behaviour of the adhesive.

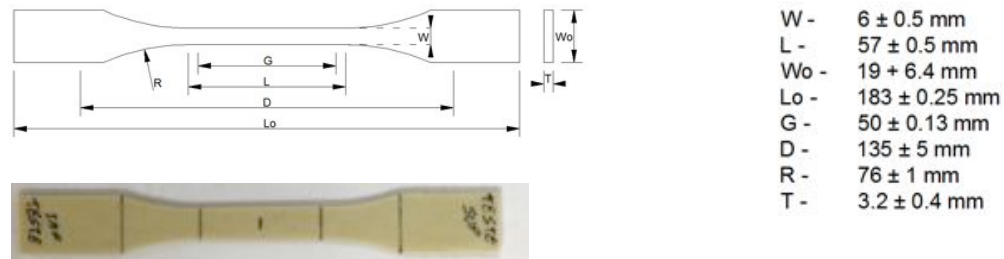
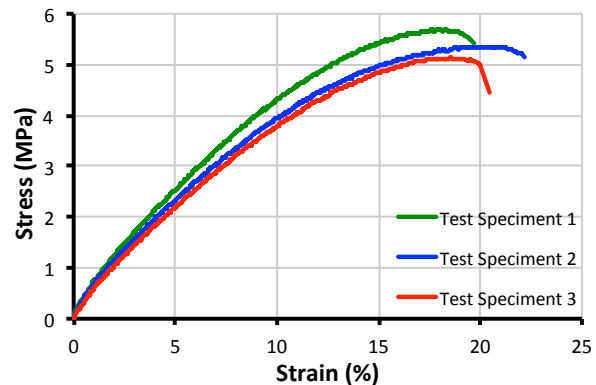


Figure 2 - Specimen geometry (Geometry type II according to ASTM D883)



(a)



(b)

Figure 3 – (a) test layout (b) results

Table 1: Uniaxial tension test results.

Specimen	σ_y [MPa]	ε_y [%]	σ_f [MPa]	ε_f [%]	Secant Modulus [MPa]	Poisson Coefficient
1	5,682	17,56	5,441	19,72	32	0,34
2	5,104	20,00	4,891	22,18	26	0,25
3	5,020	18,58	4,339	20,48	27	0,29
Average	5,268	18,71	4,891	20,79	28,30	0,29

5. FEM

Since the Uniaxial tensile tests have showed strains up to 20%, in order to simulate the material properties a large displacement theory should be considered. So, to accurately model the current adhesive, a hyperelastic rheological law should be taken into account because this type of constitutive laws are used to model materials that respond elastically when subjected to very large strains. A hyperelastic material is still an elastic material, which means it returns to its original shape after the forces have been removed. It is also Cauchy-elastic, which means that the stress is determined by the current state of deformation and not history or path of deformation [11]. The difference between linear elastic and a hyperelastic material is the fact that, in the second one, the stress-strain relation derives from a strain energy density function and not a constant factor.

The concept of a strain energy function could be described with the example of a non-linear elastic bar [8].

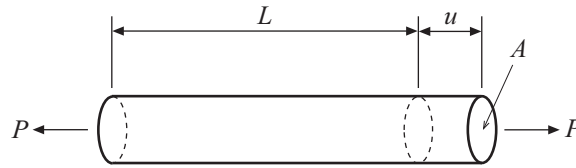


Figure 4 – non-linear elastic bar [8]

In order to analyse hyperelastic materials the conventional strain (ε) is often replaced by the so-called stretch (λ), which is defined by a quotient between the current and the original length:

$$\lambda = \frac{l_1}{l_0} = \frac{(l_1 - l_0) + l_0}{l_0} = \frac{l_0 + u}{l_0} = \varepsilon + 1$$

The strain energy density is defined as a function, $W(\lambda)$, describing the strain energy density per undeformed volume of the bar. The total strain energy, U , is thus expressed by multiplying $W(\lambda)$ with the undeformed volume:

$$U = Al_0 W(\lambda)$$

The incremental work done by the external force, F , should be equal to the increment in total strain energy. Hence, the energy balance is stated as:

$$F du = dU$$

The increment in total strain energy can be expressed by the use of $W(\lambda)$:

$$dU = A l_0 \frac{dW(\lambda)}{d\lambda} d\lambda$$

The displacement increment can also be written in terms of stretch by using:

$$\lambda = \frac{l_0 + u}{l_0} \Leftrightarrow u = (\lambda - 1) l_0$$

Differentiating u gives:

$$du = l_0 d\lambda$$

Inserting them into the energy balance equation yields

$$F l_0 d\lambda = A l_0 \frac{dW(\lambda)}{d\lambda} d\lambda \Leftrightarrow \frac{F}{A} = \frac{dW(\lambda)}{d\lambda} \Leftrightarrow \sigma_{nom} = \frac{dW}{d\lambda}$$

Based on this one-dimensional example, it is demonstrated that the stress can be obtained directly from the strain energy function. In a multi-axial case, the stresses are found in a similar manner from the strain energy density function. In that situation, the strain measured used is the left Cauchy-Green deformation tensor, B . A general assumption is that W depends on all of the components of the strain measure, giving:

$$W = W(B)$$

However, the state of deformation is fully determined by the principal stretches and the principal directions (n). In an isotropic material the three principal stretches are independent of the principal directions and consequently the strain energy density function can be written

$$W = W(\lambda_1, \lambda_2, \lambda_3, n_1, n_2, n_3) = W(\lambda_1, \lambda_2, \lambda_3)$$

In order to obtain the principal stretches it is necessary to find the roots of the characteristic polynomial of B . Since it is easier to obtain the coefficients of the characteristic polynomial, instead of using the principal stretches we could therefore express W as function of the strain invariants, where J is the volume ratio.

$$\begin{aligned} W &= W(I_1, I_2, I_3) \\ \left\{ \begin{aligned} I_1 &= \text{tr}(B) = \lambda_1^2 + \lambda_2^2 + \lambda_3^2 \\ I_2 &= \frac{1}{2}(\text{tr}(B)^2 - \text{tr}(B^2)) = \lambda_1^2 \lambda_2^2 + \lambda_1^2 \lambda_3^2 + \lambda_2^2 \lambda_3^2 \\ I_3 &= \det(B) = \lambda_1^2 \lambda_2^2 \lambda_3^2 = J^2 \end{aligned} \right. \end{aligned}$$

For nearly incompressible materials, a more convenient set of invariants of B could be used, since the deviatoric (W_d) and the volumetric (W_v) terms of the strain energy function are split. As a result, W_d is the

strain energy necessary to change the shape and W_V is the strain energy necessary to change the volume, so under a pure volume change, I_1 and I_2 remain constant.

$$\begin{cases} \bar{I}_1 = J^{-\frac{2}{3}} I_1 \\ \bar{I}_2 = J^{-\frac{4}{3}} I_2 \\ \bar{I}_3 = \sqrt{\det(B)} = 1 \end{cases}$$

Therefore, the stress-strain law for an isotropic hyperelastic material could be derived from the strain energy density function considering an energy balance equation in the same way as in the initial example of the elastic bar [8,10]. The results are derived below [10]:

- Strain energy density in terms of I_1, I_2, I_3

$$\sigma_{ij} = \frac{2}{\sqrt{I_3}} \left[\left(\frac{\partial U}{\partial I_1} + I_1 \frac{\partial U}{\partial I_2} \right) B_{ij} - \frac{\partial U}{\partial I_2} B_{ik} B_{kj} \right] + 2\sqrt{I_3} \frac{\partial U}{\partial I_3} \delta_{ij}$$

- Strain energy density in terms of \bar{I}_1, \bar{I}_2, J

$$\sigma_{ij} = \frac{2}{J} \left[\frac{1}{J^{2/3}} \left(\frac{\partial \bar{U}}{\partial \bar{I}_1} + \bar{I}_1 \frac{\partial \bar{U}}{\partial \bar{I}_2} \right) B_{ij} - \left(\bar{I}_1 \frac{\partial \bar{U}}{\partial \bar{I}_1} + 2\bar{I}_2 \frac{\partial \bar{U}}{\partial \bar{I}_2} \right) \frac{\delta_{ij}}{3} - \frac{1}{J^{4/3}} \frac{\partial \bar{U}}{\partial \bar{I}_2} B_{ik} B_{kj} \right] + \frac{\partial \bar{U}}{J} \delta_{ij}$$

The present work takes into account different rheological models, which could be classified accordingly to the form of the strain energy function. Most of the hyperelastic constitutive models can be grouped in two broad categories: phenomenological and micromechanical models, see Figure 5. Since the physical significance of micro-mechanical material constants is often unclear, the use of phenomenological model is suggested.

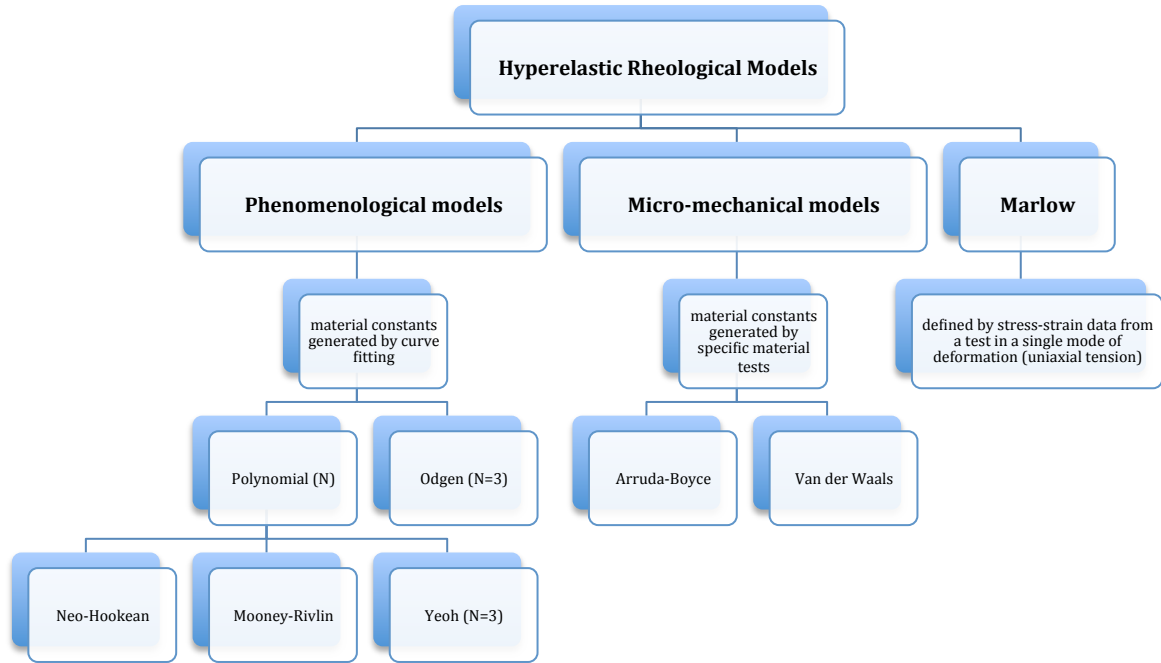


Figure 5 - Hyperelastic Rheological models

A general form of a strain energy density function, implemented not only in ABAQUS but also in most of the finite element software's is the polynomial form, given by the following series expansion (C_{ij} are unknown constants):

$$U = \sum_{i+j=1}^N C_{ij} (\bar{I}_1 - 3)^i (\bar{I}_2 - 3)^j + \sum_{i=1}^N \frac{1}{D_i} (J^{el} - 1)^{2i}$$

The sum is formally written as a sum to infinity but, usually, only a few terms are considered:

$$U = C_{10}(\bar{I}_1 - 3) + C_{01}(\bar{I}_2 - 3) + C_{20}(\bar{I}_1 - 3)^2 + C_{11}(\bar{I}_1 - 3)(\bar{I}_2 - 3) + C_{02}(\bar{I}_2 - 3)^2 + C_{30}(\bar{I}_1 - 3)^3 \\ + C_{21}(\bar{I}_1 - 3)^2(\bar{I}_2 - 3) + C_{12}(\bar{I}_1 - 3)(\bar{I}_2 - 3)^2 + C_{03}(\bar{I}_2 - 3)^3 + \dots + \sum_{i=1}^N \frac{1}{D_i} (J^{el} - 1)^{2i}$$

Regardless of the value of N, the initial shear modulus (μ_0) and the initial bulk modulus (k_0) depend only on the polynomial coefficients of the first order (N=1).

$$\mu_0 = 2(C_{10} + C_{01})$$

$$k_0 = \frac{2}{D_1}$$

- **Neo-Hookean**

Taking only the first term in the series yields to the neo-Hooke form, which was first derived from statistical mechanics by considering the molecular structure of rubbers. [3,19]

$$U = C_{10}(\bar{I}_1 - 3) + \frac{1}{D_1} (J^{el} - 1)^2$$

- **Mooney-Rivlin**

If only the linear terms in the deviatoric strain energy are retained (N=1), the Mooney-Rivlin is obtained:

$$U = C_{10}(\bar{I}_1 - 3) + C_{01}(\bar{I}_2 - 3) + \frac{1}{D_1}(J^{el} - 1)^2$$

The Mooney-Rivlin form can be viewed as an extension of the Neo-Hookean form, where a term that depends on the second invariant of the left Cauchy-Green tensor is added.

- **Yeoh**

By setting specific coefficients to zero, particular forms of the polynomial function could be obtained. The reduced polynomial form is obtained if all C_{ij} with $j \neq 0$ are set to zero. The Yeoh form is a special case of the reduced polynomial with N=3 and it depends only on the first strain invariant.

$$U = C_{10}(\bar{I}_1 - 3) + C_{20}(\bar{I}_1 - 3)^2 + C_{30}(\bar{I}_1 - 3)^3 + \frac{1}{D_1}(J^{el} - 1)^2 + \frac{1}{D_2}(J^{el} - 1)^4 + \frac{1}{D_3}(J^{el} - 1)^6$$

- **Ogden**

The Ogden model expresses the strain energy function in terms of principal stretches and it cannot be compared with the polynomial form, except for a specific choice of constants.

$$U = \sum_{i=1}^N \frac{2\mu_i}{\alpha_i^2} (\bar{\lambda}_1^{\alpha_i} + \bar{\lambda}_2^{\alpha_i} + \bar{\lambda}_3^{\alpha_i} - 3) + \sum_{i=1}^N \frac{1}{D_i} (J^{el} - 1)^{2i}$$

For N=1 and $\alpha_1 = 2$ the Neo-Hook model is obtained and for N=2, $\alpha_1 = 2$ and $\alpha_2 = 2$ the Mooney-Rivlin model is obtained. The initial bulk modulus, k_0 , depends on D_1 as before and the initial shear modulus, μ_0 , depends on all coefficients: $\mu_0 = \sum_{i=1}^N \mu_i$.

- **Arruda-Boyce**

The Arruda-Boyce potential depends only on the first invariant and it is based on statistical mechanics.

$$U = \mu \left\{ \frac{1}{2}(\bar{I}_1 - 3) + \frac{1}{20\lambda_m^2}(\bar{I}_1^2 - 9) + \frac{11}{1050\lambda_m^4}(\bar{I}_1^3 - 27) + \frac{19}{7000\lambda_m^6}(\bar{I}_1^4 - 81) + \frac{519}{673750\lambda_m^8}(\bar{I}_1^5 - 243) \right\} + \frac{1}{D} \left(\frac{J_{el}^2 - 1}{2} - \ln(J_{el}) \right)$$

The material coefficients have physical meaning, μ is the initial shear modulus, λ_m is the locking stretch, which is the stretch at which stress starts to increase without limit and $D=2/K_0$ is the incompressibility parameter. If λ_m tends to infinite, the Arruda-Boyce form becomes the Neo-Hookean form.

- **Van der Waals**

The Van der Waals potential, also known as the Kilian model, has the following form:

$$U = \mu \left\{ -(\lambda_m^2 - 3)[\ln(1 - \eta) + \eta] - \frac{2}{3}a \left(\frac{I - 3}{2} \right)^{\frac{3}{2}} \right\} + \frac{1}{D} \left(\frac{J_{el}^2 - 1}{2} - \ln(J_{el}) \right)$$

In contrast to the Arruda-Boyce model the mathematical structure of the Van der Waals potential is such that the strain energy tends to infinity as the locking stretch is reached. Thus, stretches larger than the locking stretch cannot be used in the Van der Waals potential.

- **Marlow**

The form of the Marlow strain energy potential is:

$$U = U_{dev}(\bar{I}_1) + U_{vol}(J^{el})$$

According to Abaqus [3], the deviatoric part of the potential is defined by providing either uniaxial, equibiaxial, or planar test data, while the volumetric part is defined by providing the respective lateral strains data, or by giving data from a volumetric test, or by defining a Poisson's ratio.

5.1. Uniaxial tension test

A 3D model of the dumbbell shaped specimen was created. The boundary conditions imposed to the FEM model were encastrate on the lower and widest part and, at the top of the specimen, a load was applied in the surfaces which are in contact with the upper claw of the testing machine. A minimum of 3 elements through the thickness was considered.

In the stretching simulation, since the use of “hybrid” (mixed formulation) elements is recommended in both incompressible and almost incompressible cases, 8-node linear brick hybrid elements (C3D8H) were used to mesh the 3D-model.

The displacement and strain values along the axial direction in the central section of specimen were compared with the experimental data.

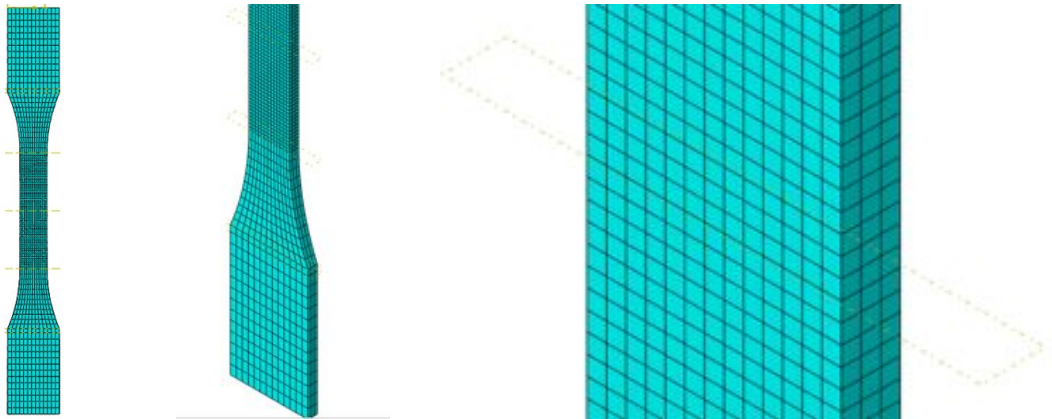


Figure 6 – Uniaxial tension model

Stress-strain data from experimental results were imported into Abaqus and the numerical fitting was performed considering several strain energy functions implemented in that finite element package. Since only uniaxial test data were available, a Poisson coefficient of 0.3 was considered. Table 3 lists the coefficients obtained from the fitting procedure.

Neo Hooke	C_{10}	7,22563419
	D_1	0,063875149
	C_{01}	0
Yeoh	C_{10}	9,25161515
	C_{20}	-47,6971078
	C_{30}	232,349435
	D_1	0,049887339
	D_2	0
	D_3	0
Mooney-Rivlin	C_{10}	-15,3353613
	C_{01}	24,7136111
	D_1	0,04921371
Polynomial (N=2)	C_{10}	-176,118162
	C_{01}	188,670357
	C_{20}	8488,60299
	C_{11}	-20045,3507
	C_{02}	11998,9902
	D_1	0,036769541
	D_2	0
Odgen (N=3)	μ_1	-388,179675
	α_1	-3,83103856
	μ_1	195,117036
	α_2	-3,73751909
	μ_3	215,416295
	α_1	-5,97308164
	D_1	0,041294225
	D_2	0
	D_3	0
Arruda-Boyce	μ	14,4512525
	λ_m	572,257168
	D	0,063875102
	μ_0	14,4512789
Van der Waals	μ	19,5169585
	λ_m	9,94927816
	a	2,31878865
	BETA	0
	D	0,092778281

Table 3 - Coefficients obtained for each strain energy potential through the fitting procedure

When calibrated with uniaxial tension data, the fitting for small and large strains of the Mooney-Rivlin, the Polynomial (N= 2), the Odgen and the Van der Waals material models is very satisfactory.

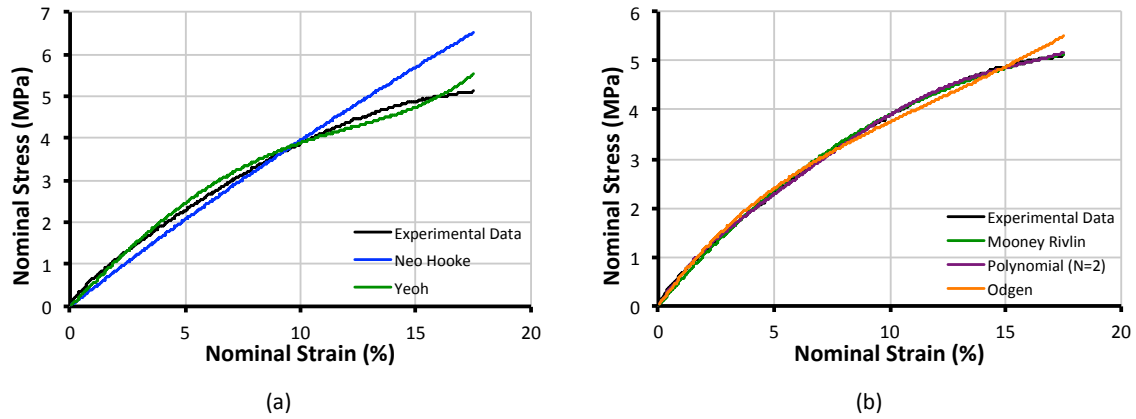


Figure 7 – Numerical Fitting for the (a) reduced polynomial (b) polynomial and Odgen strain energy functions

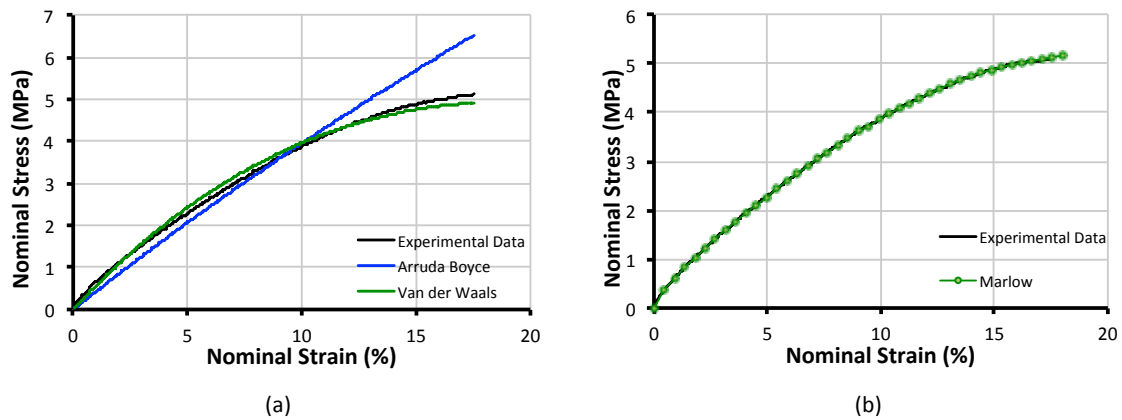


Figure 8 - Numerical Fitting for the (a) Arruda-Boyce, Van der Waals and (b) Marlow strain energy functions

Results and Discussion

After the numerical fitting procedure and using the coefficients obtained, a FEA was prepared. The results show that with the Mooney-Rivlin, the Polynomial (N= 2), the Odgen and also with the Van der Waals material models the agreement between numerical and experimental is very satisfactory.

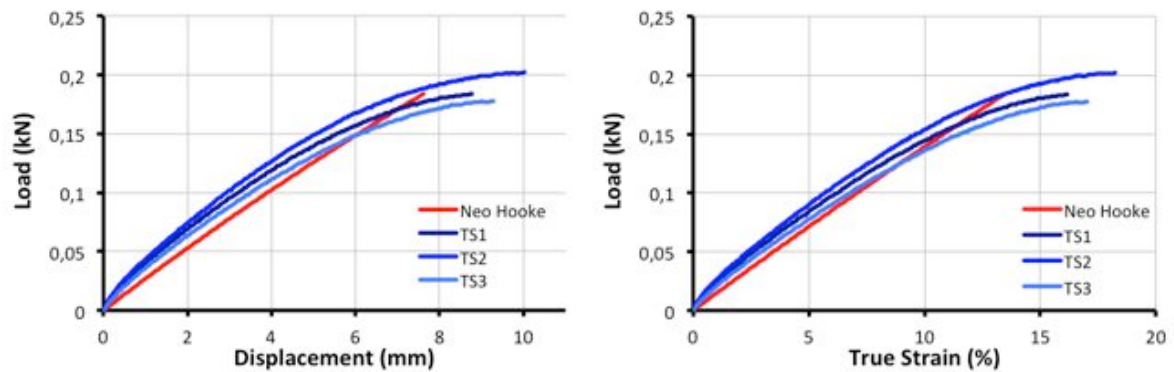


Figure 9 –Neo-Hooke model

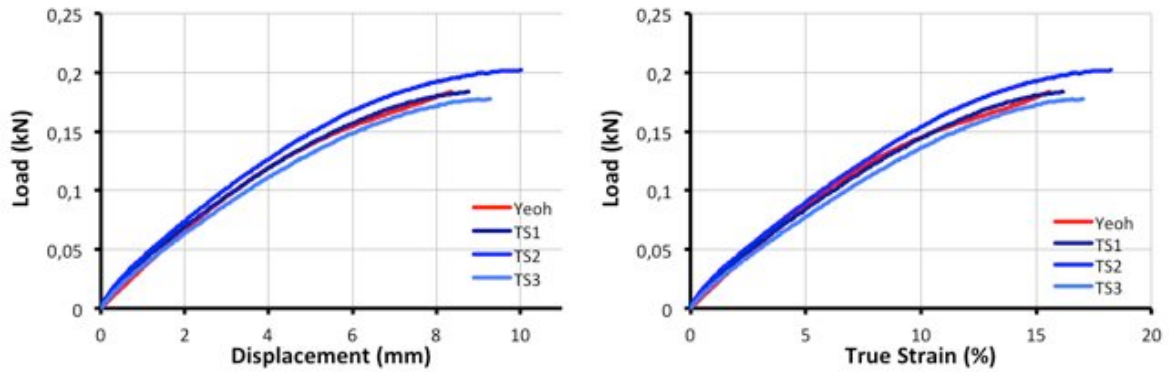


Figure 10 –Yeoh model

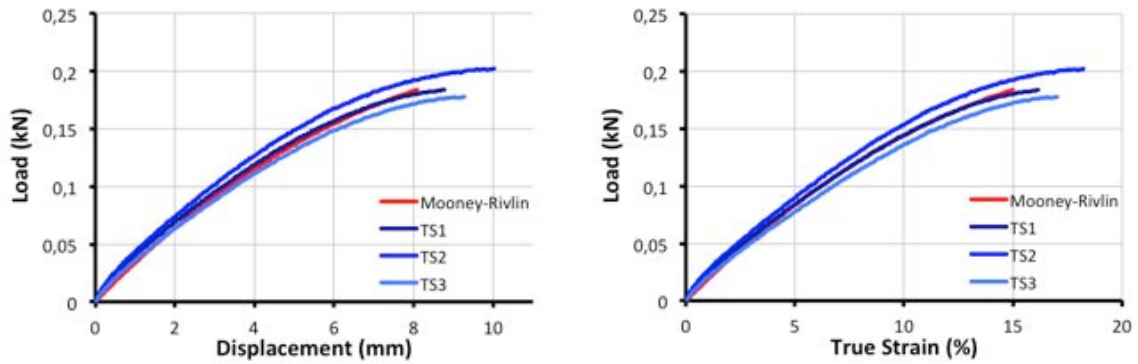


Figure 11 –Mooney-Rivlin model

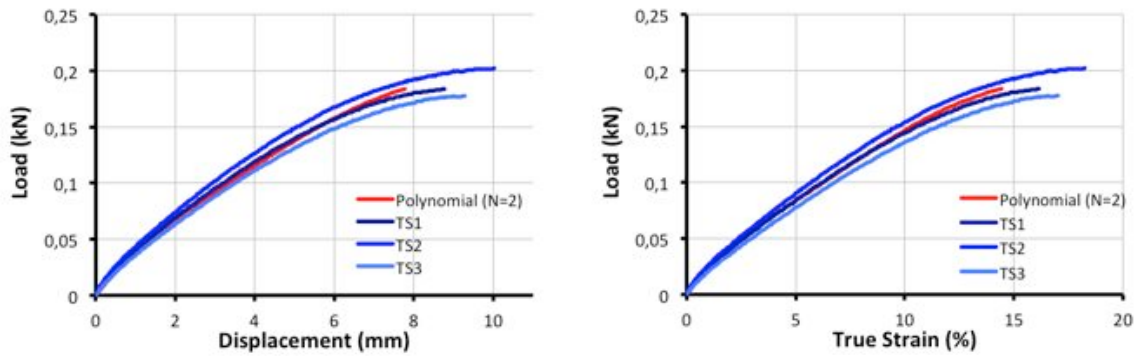


Figure 12 –Polynomial (N=2) model

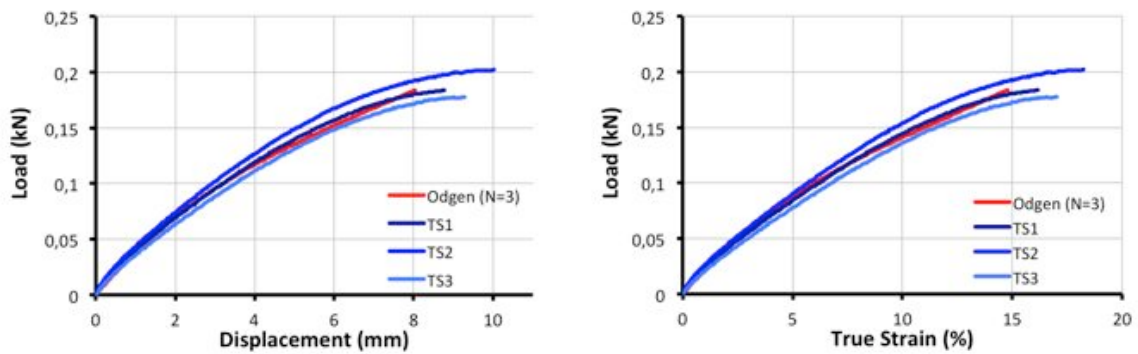


Figure 13 –Odgen model

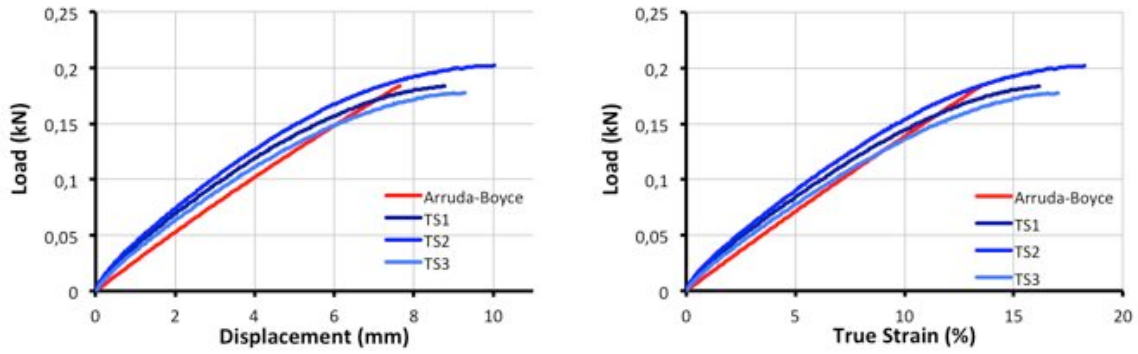


Figure 14 –Arruda-Boyce Model

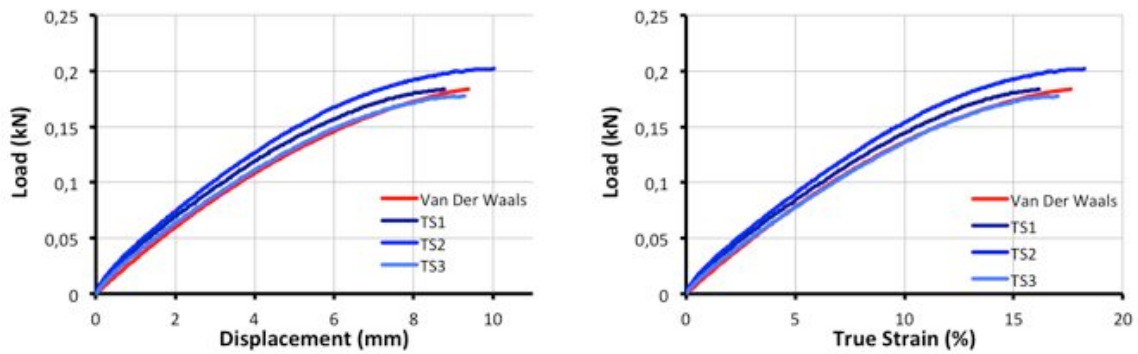


Figure 15 – Van der Waals model

Note: For the Marlow model, numerical convergence was not achieved.

The Poisson coefficient used was calculated according to the exposed in the ASTM 638, based on a relation between the transversal and longitudinal strains at low strains. However, as these types of materials are often considered incompressible or nearly so, the models were re-calculated with the assumption of no volumetric change ($\nu=0.5$). All of the coefficients calculated from the fitting procedure are same, except for the volumetric terms. In this case, all of these values (D_i) were set to 0.

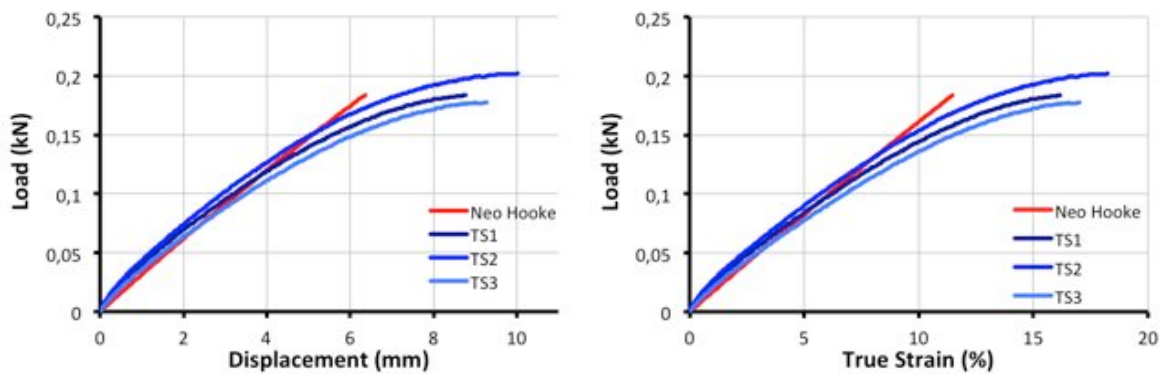


Figure 16 –Neo-Hooke model

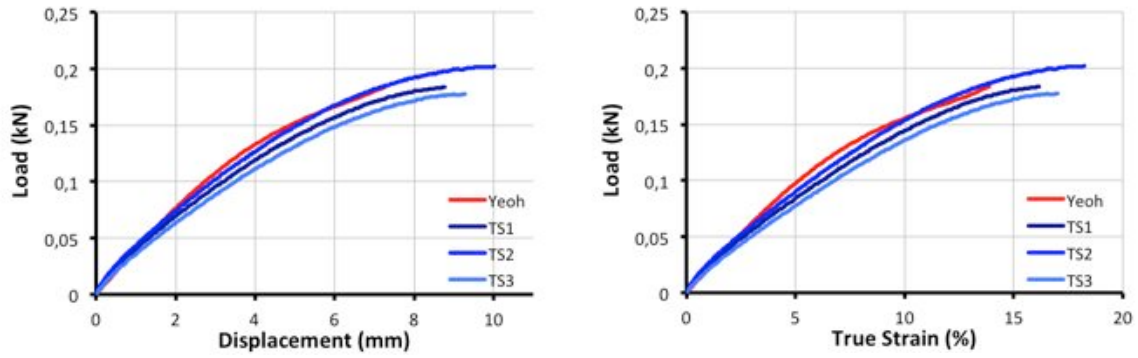


Figure 17 –Yeoh model

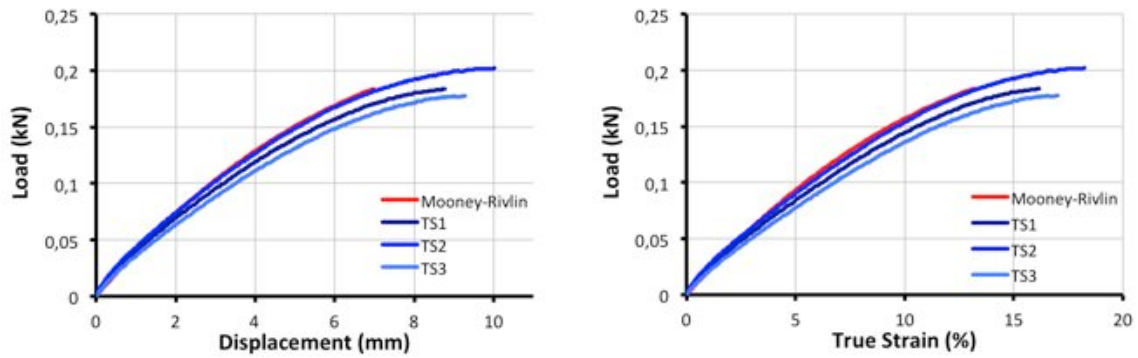


Figure 18 –Mooney-Rivlin model

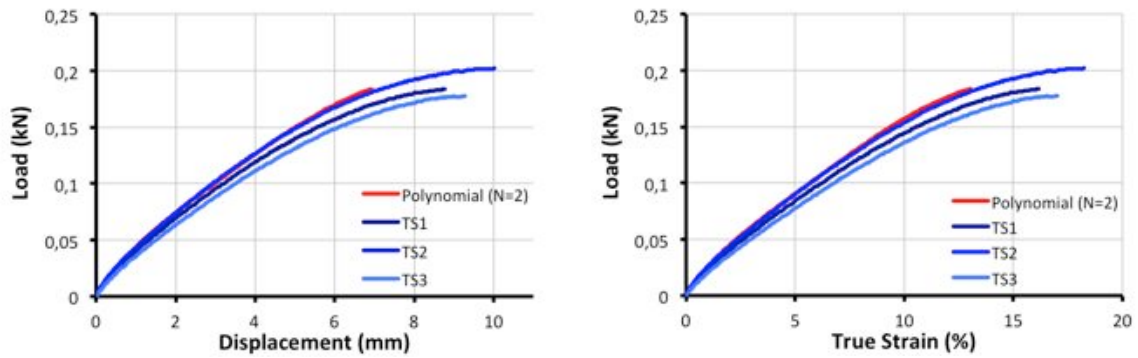


Figure 19 –Polynomial (N=2) model

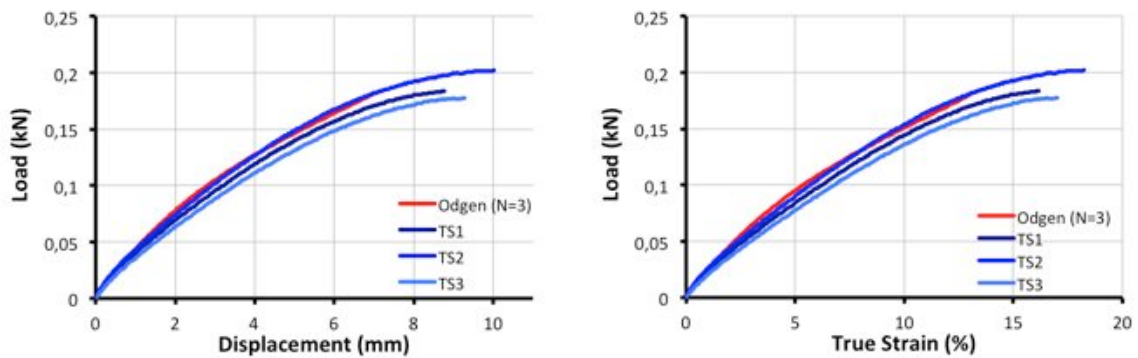


Figure 20 –Odgen model

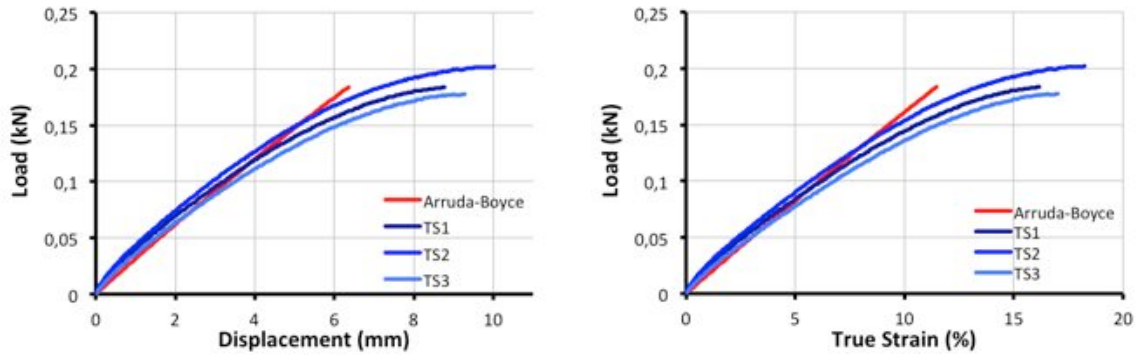


Figure 21 –Arruda-Boyce Model

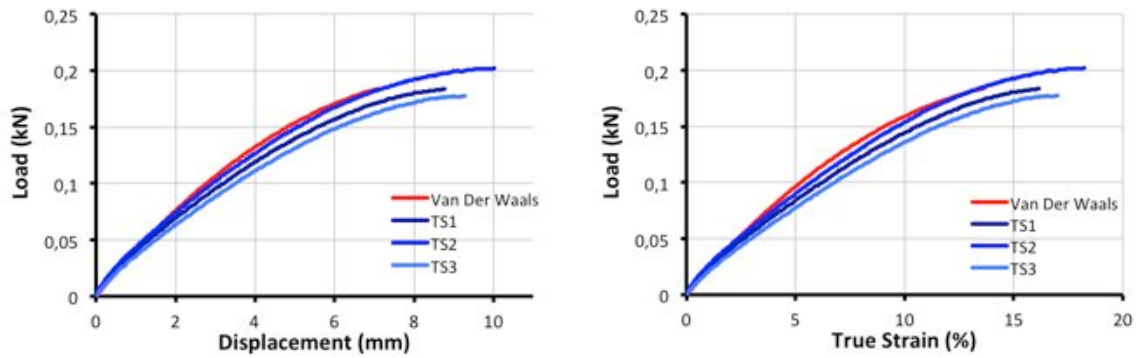


Figure 22 – Van der Waals model

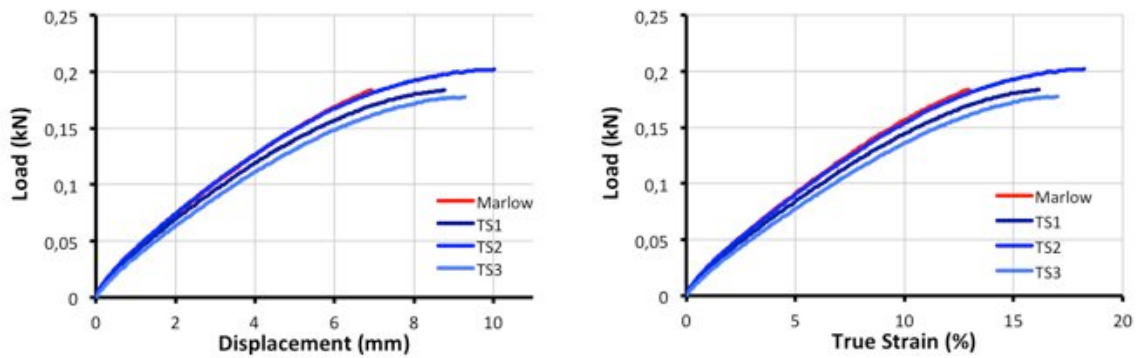


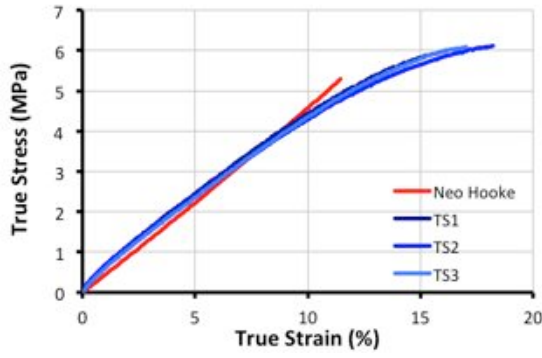
Figure 23 – Marlow model

As it was considered an incompressible material, the nominal stress - nominal strain curve obtained in the experimental tests can be converted to a true stress - true strain curve using the following expressions:

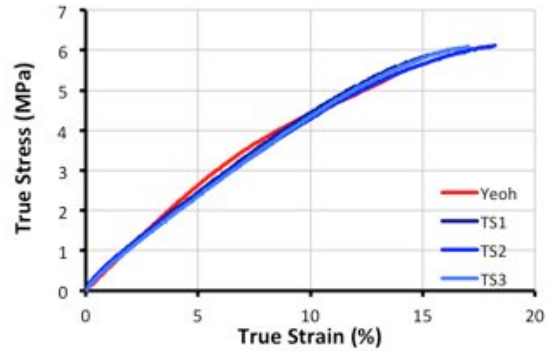
$$\sigma = S(1+e)$$

$$\epsilon = \ln(1+e)$$

where σ : true stress
 S : Engineering Stress
 ϵ : true strain
 e : Engineering Strain

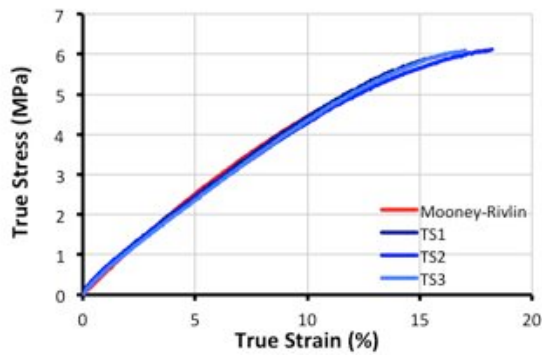


(a)

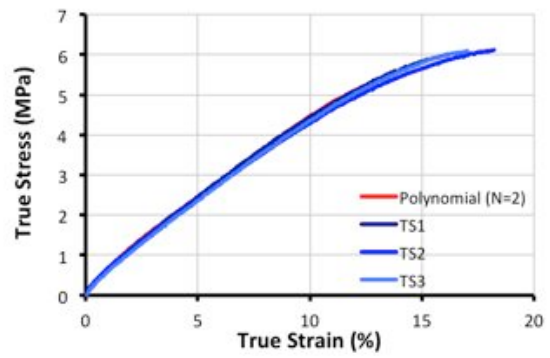


(b)

Figure 24 – True Stress vs True Strain results (a) Neo-Hooke model (b) Yeoh model

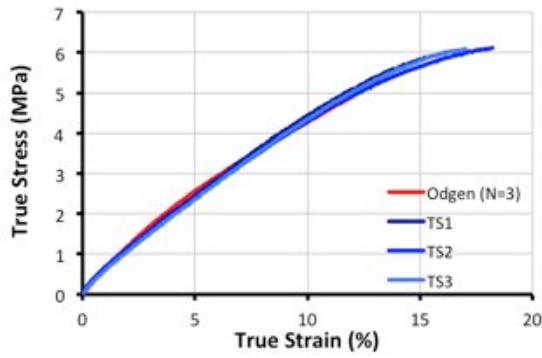


(a)

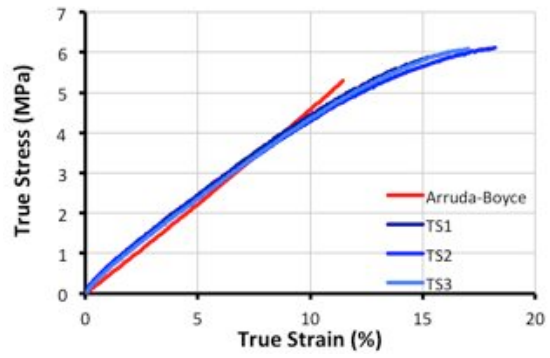


(b)

Figure 25 - True Stress vs True Strain results (a) Mooney-Rivlin model (b) Polynomial (N=2) model



(a)



(b)

Figure 26 – True Stress vs True Strain results (a) Odgen model (b) Arruda-Boyce model

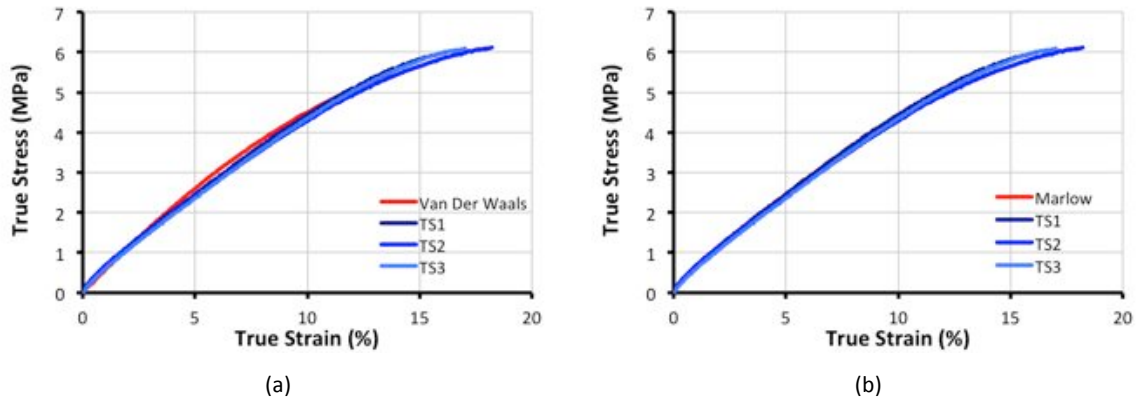
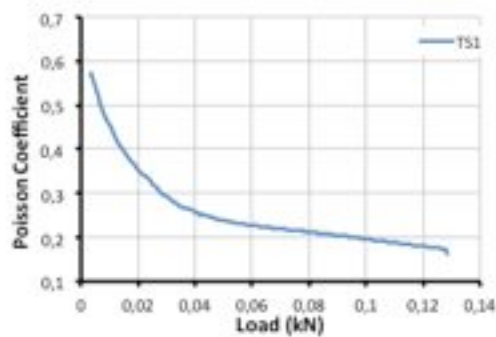


Figure 27 - True Stress vs True Strain results (a) Van der Waals model (b) Marlow model

Considering a Poisson coefficient of 0,5, there is also a good agreement between the numerical models and the experimental data especially for the following models: Mooney-Rivlin, Polynomial (N= 2), Odgen, Van der Waals and Marlow. However, compared with the previous case, the models are a little bit stiffer. For the ultimate load, the displacement is getting far from the registered experimentally. Because of this uncertainty about the Poisson coefficient, based on the values obtained from electric strain gauges placed in the test specimens, a relation between the axial strains and the load were explored.



It is noticed that the transversal and longitudinal relation is not constant, and when the axial strain limit of the strain gauges was reached, the Poisson coefficient tend to be approximately 0,16. Due to this fact, new calculations were performed considering new volumetric terms:

Neo-Hooke	D_1	0,121693172
Yeoh	D_1	0,095043982
	D_2	0
	D_3	0
Mooney-Rivlin	D_1	0,093760602
Polynomial (N=2)	D_1	0,070052316
	D_2	0
Odgen (N=3)	D_1	0,078672619
	D_2	0
	D_3	0
Arruda-Boyce	D	0,121693083
Van der Waals	D	0,176758621

Table 4 - New volumetric terms considered

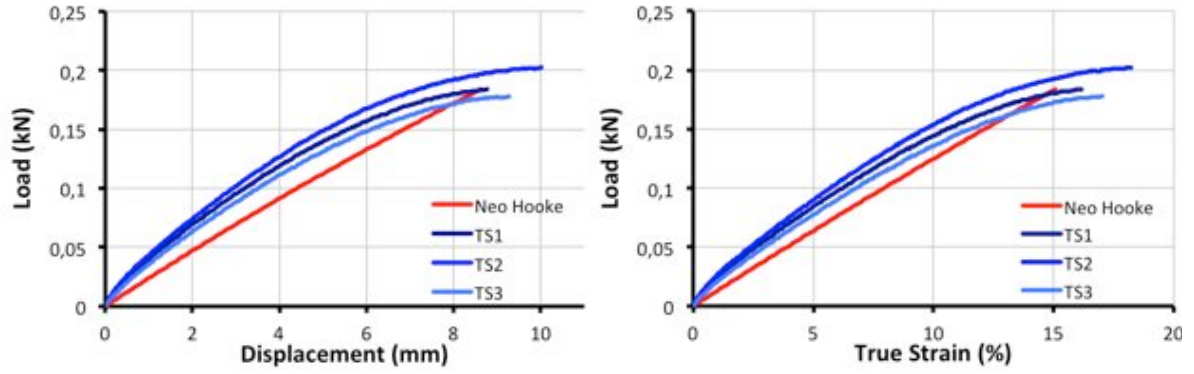


Figure 28 – Neo-Hookean model

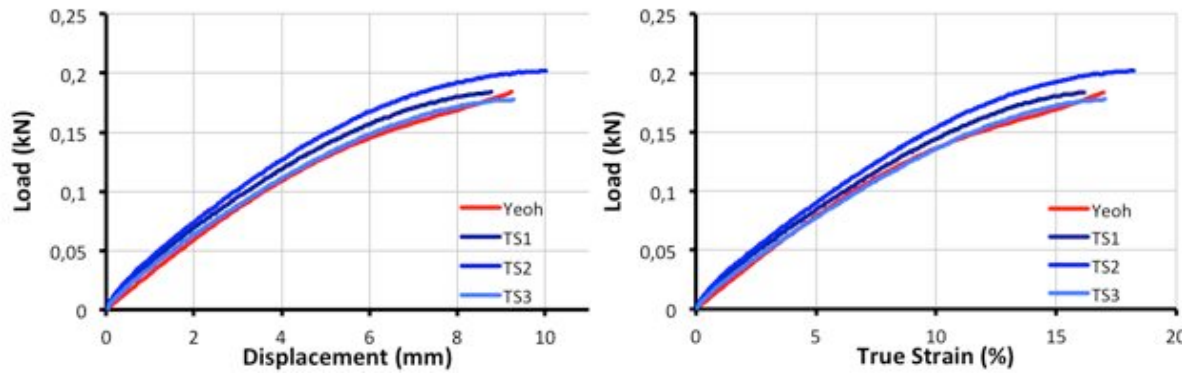


Figure 29 – Yeoh model

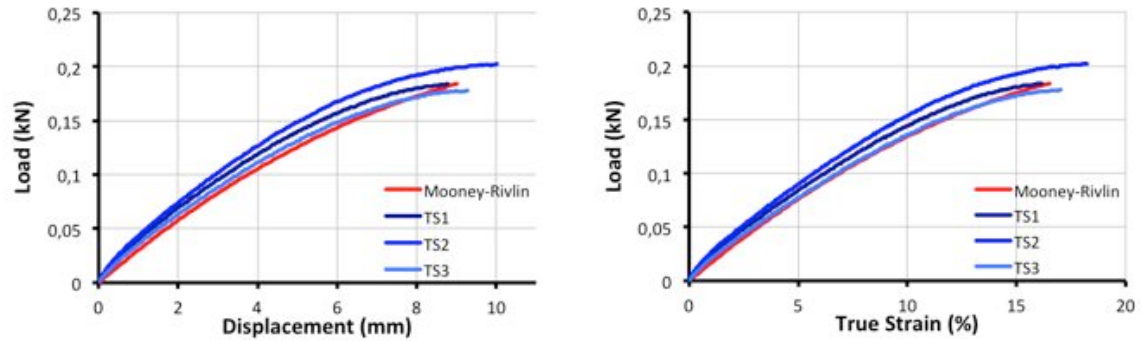


Figure 30 – Mooney-Rivlin model

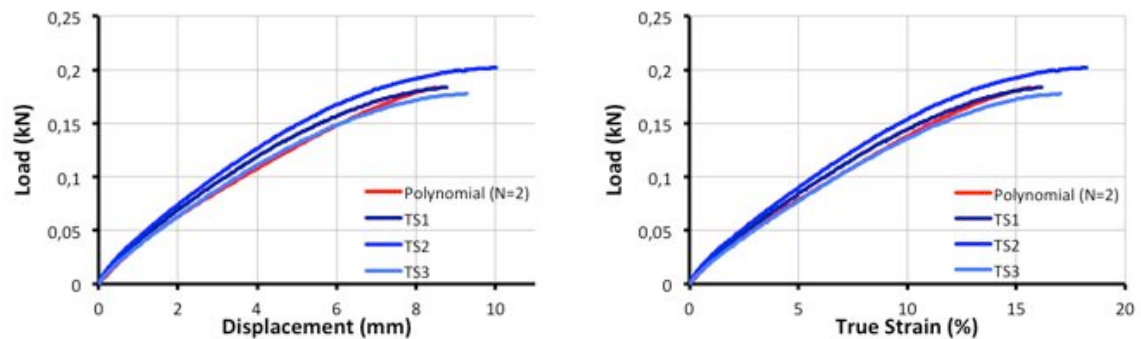


Figure 31 – Polynomial (N=2) model

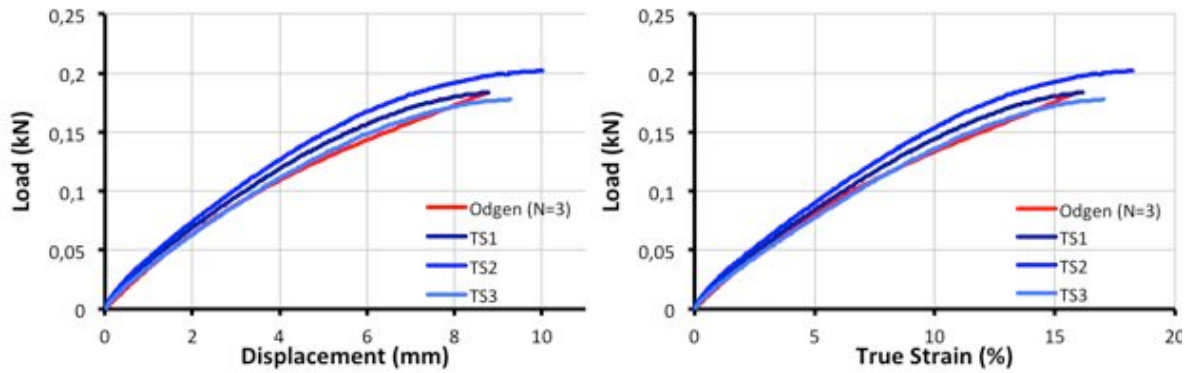


Figure 32 – Odgen model

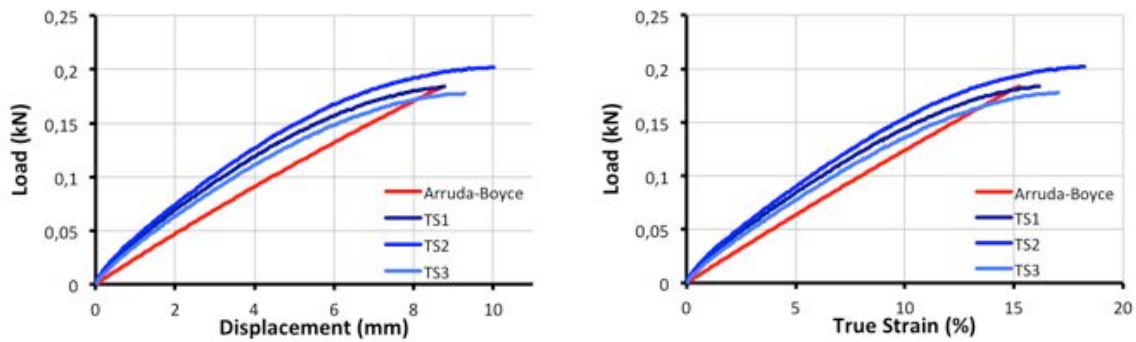


Figure 33 – Arruda-Boyce model

Note: For the Van der Waals and for the Marlow model numerical convergence was not achieved.

The results show that considering a Poisson Coefficient of 0.16, the models are more flexible and the ones that best fit the experimental data are, by order:

1. The polynomial (N=2);
2. The Odgen;
3. The Mooney-Rivlin;
4. Yeoh;

However, despite of the agreement to the experimental curves is not as good as when a Poisson coefficient of 0.3 is chosen, the ultimate displacement verified is very similar to experimental recorded. This could mean that the ASTM 638 recommendation to evaluate the Poisson coefficient might not be so correct for this particular material. So, in order to overcome this uncertainty, additional experimental tests should be made in order to characterize the volumetric parameters of the adhesive.

The following step was to apply the calibrated properties of these models to a different kind of solicitation (shear) and evaluate if they suitable or not to represent the behaviour of the adhesive layer.

5.2. Tension + shear

This numerical model tries to simulate a push-out shear test done on two test specimens. The objective is to evaluate if the constitutive laws considered in the uniaxial tension models are still suitable in a shear plus tension load case.

- Layout and geometry

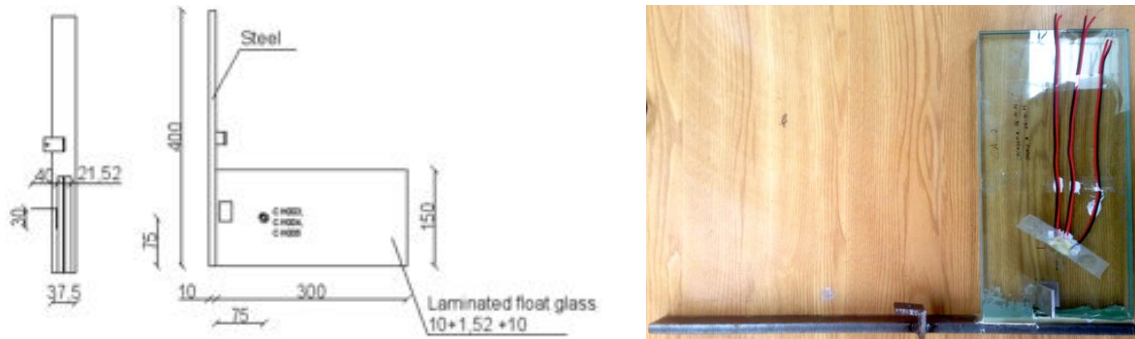


Figure 34 - test specimen geometry

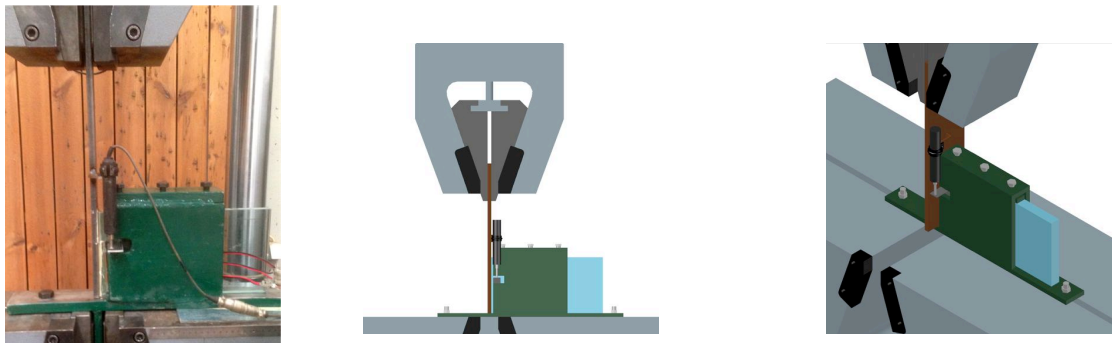


Figure 35 - layout

- Properties

Different strain energy potentials were applied to the adhesive layer in order to see which one fits the best the experimental data. The properties used to model the other elements could be consulted in the following table.

Element	Elasticity Modulus	Poisson Coefficient
Float Glass	70 000 MPa	0.23
SentryGlas Plus	300 MPa	≈ 0.5
Steel	210 000 MPa	0.3

Table 5 - Properties considered in FEM

- Boundary Conditions

The boundary conditions considered were fixed at the bottom of the glass. Transversal displacements were also restrained according to the test setup, see Figure 36.



Figure 36 - FEM: Boundary Conditions

- Load Strategy

In order to represent exactly the experiment, the load was applied in two steps:

- 1) Bolt loads are applied vertically at the top of the glass against a steel bar, which will help the system to restrain the glass. Therefore, in the following step, a relative displacement in the adhesive layer might happen;
- 2) After the bolt loads are applied, the steel bar position is fixed in the model and the vertical load, F is applied at the top of the steel part;

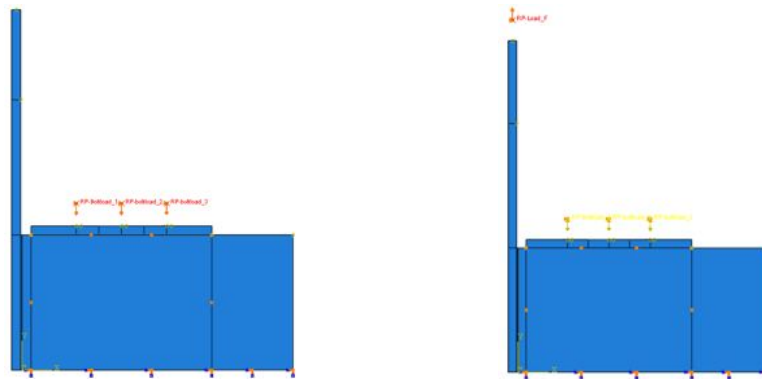


Figure 37 - FEM: Load steps

- Interactions

To model the interactions between the elements, a tie constraint was considered. In the contact pairs, the adhesive was always the slave surface because it has got the densest mesh and the other materials are stiffer.

- Mesh

In the adhesive layer, C3DH8 elements were considered. The joint has 4 elements in the thickness and 30 through the height of the connection. To the remaining materials, C3D8 elements were implemented with an element size of approximately 5mm.

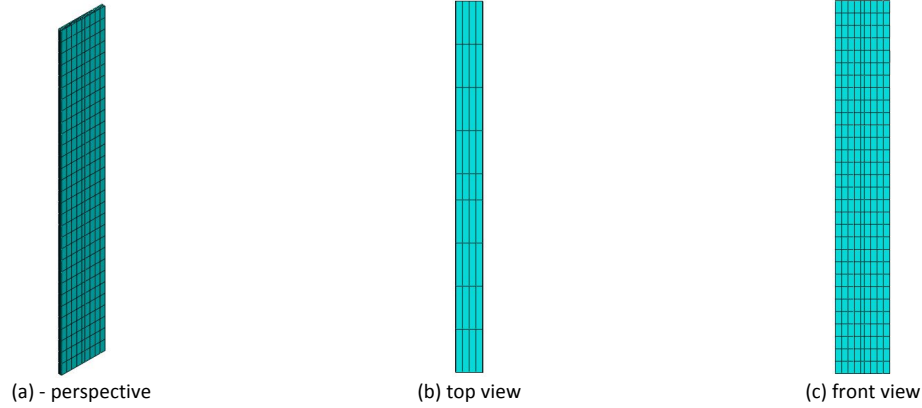


Figure 38 - FEM: Mesh of the adhesive layer

- Results

Note: The Van der Waals and the Marlow model did not achieve numerical convergence.

At the end of the first step, the numerical stress in the glass was compared with the strain gauges values.

	TS1		TS2	
	Experimental	Numerical	Experimental	Numerical
s_{11} (MPa)	0,3997	0,149507	0,4662	0,222029
s_{22} (MPa)	-1,7997	-1,79804	-2,6663	-2,6643
Load (kN)	-	-2,22	-	-3,29

The numerical bolt loads applied at the top of the glass were causing almost the same stress state registered in the experiment. Because of that, it was decided to go to the next step.

The results, in terms of load vs displacement and shear stress vs shear strain are presented in the following figures considering a Poisson Coefficient of 0.3 and 0.16, respectively. In both cases, the agreement between the numerical output and experimental data is very bad. Despite the fact of the models with a smaller Poisson coefficient have showed a more flexible behaviour, the deformation shape is far from the observed. The Polynomial and the Mooney-Rivlin models, which used to have a good agreement between the numerical and the experimental data, have completely changed their form.

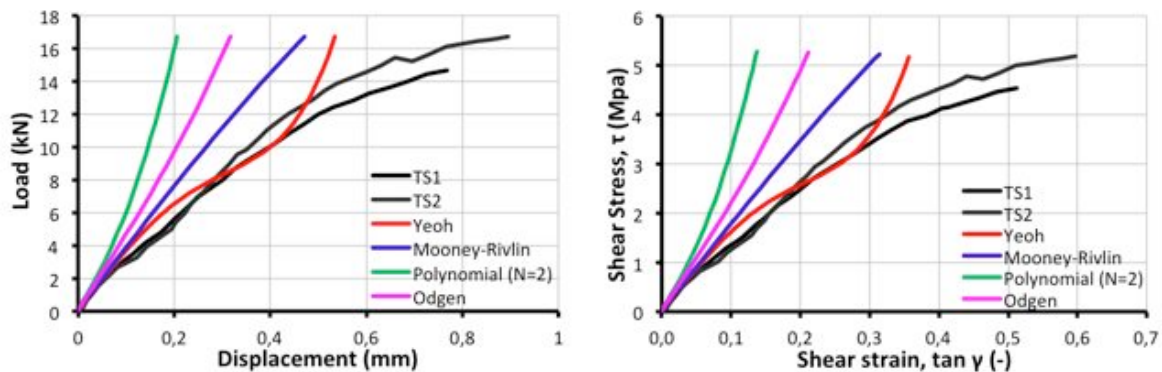


Figure 39 – Numerical vs Experimental results. Poisson Coefficient of 0.3;

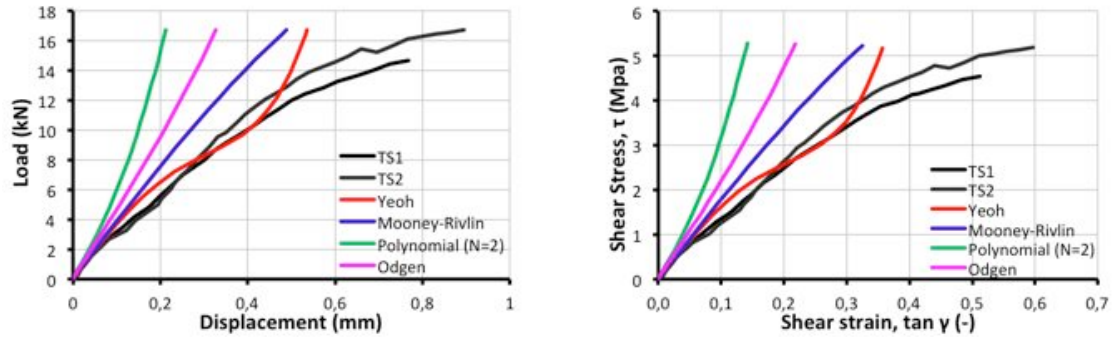


Figure 40 – Numerical vs Experimental results. Poisson Coefficient of 0.16;

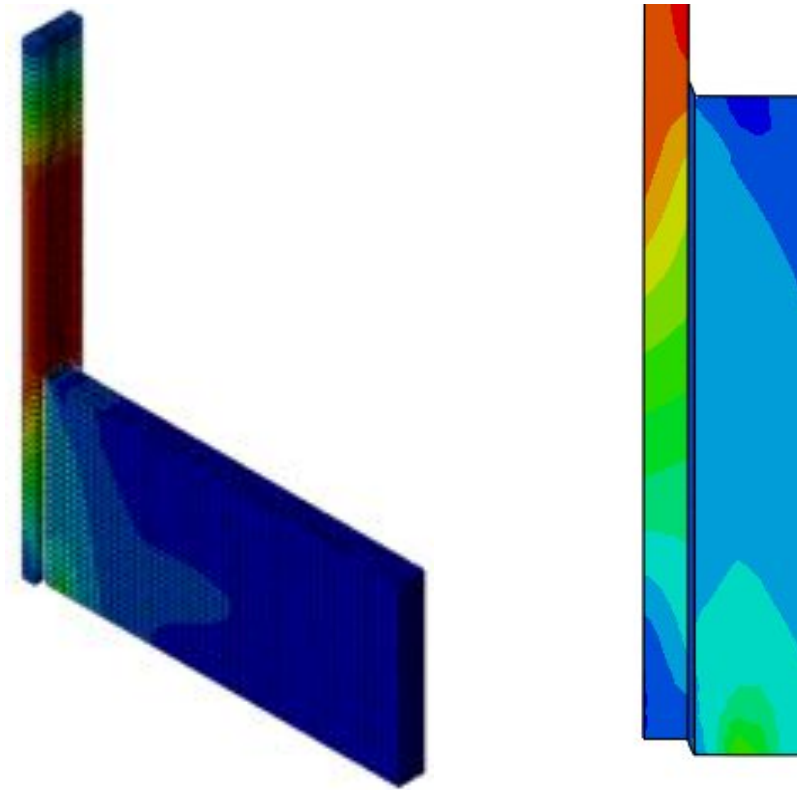


Figure 41 - FEM: deformed view (vertical scale x10)

5.3. Simple shear

The following numerical model attempts to simulate a simple shear test. The objective is to evaluate if the constitutive laws obtained through the calibration of the uniaxial tension models are still suitable in a shear state.

-

- Properties

- Boundary Conditions

- Load Strategy

Using a coupling constraint, the vertical load was applied on the steel area corresponding to the upper claw of the testing machine.



Figure 44 - FEM: Load steps

- Interactions

The interactions were modelled considering tie constraints. Due to the same reason as the previous model, the adhesive were always considered as the slave surface.

- Mesh

Adhesive layer:

- C3DH8 elements;
- Thickness: 4 elements;
- Height: 20 elements;

Remaining materials:

- C3D8 elements
- Element size of approximately 5mm.

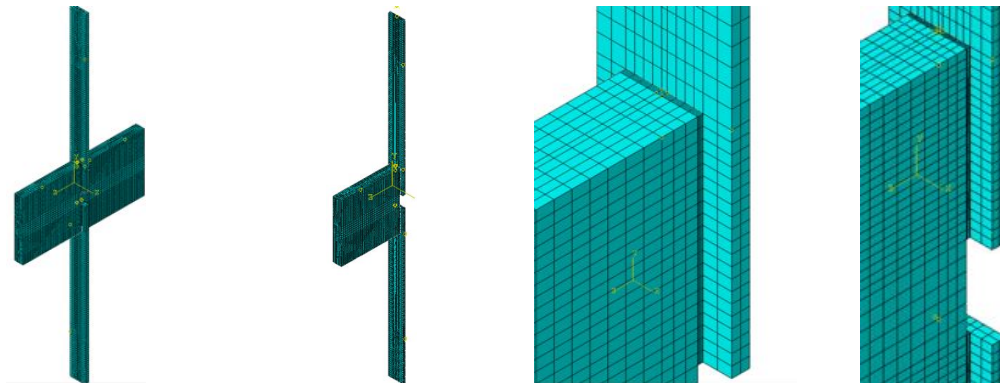


Figure 45 - FEM: Mesh adopted

- Results

Note: The Mooney-Rivlin, the Van der Waals and the Marlow model did not achieve numerical convergence so their results will not be presented.

The results, in terms of load vs displacement are presented in the following figures considering a Poisson Coefficient of 0.3 and 0.16, respectively. In both cases, the agreement between the numerical output and experimental data is again very bad.

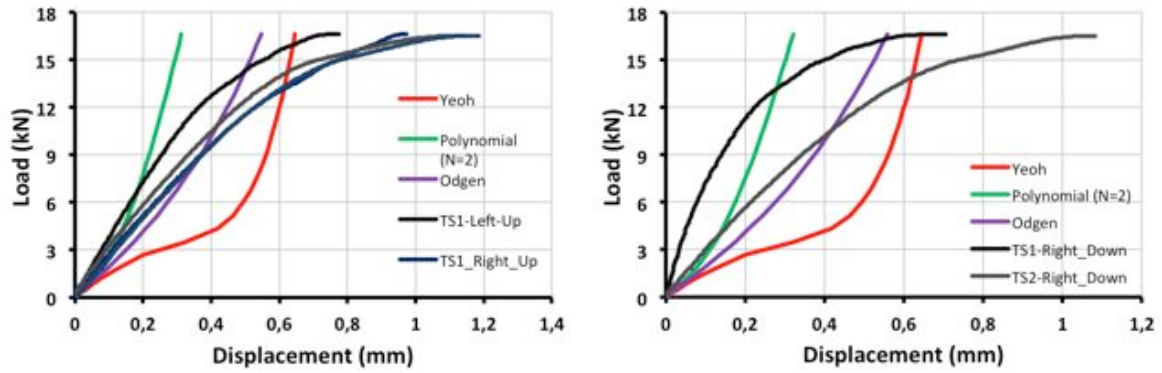


Figure 46 – Numerical vs Experimental results. Poisson Coefficient of 0.3;

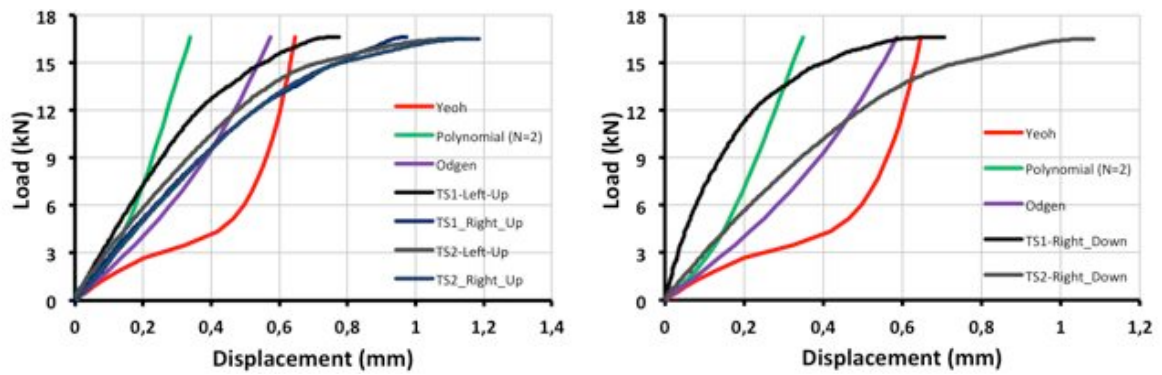


Figure 47 – Numerical vs Experimental results. Poisson Coefficient of 0.16;

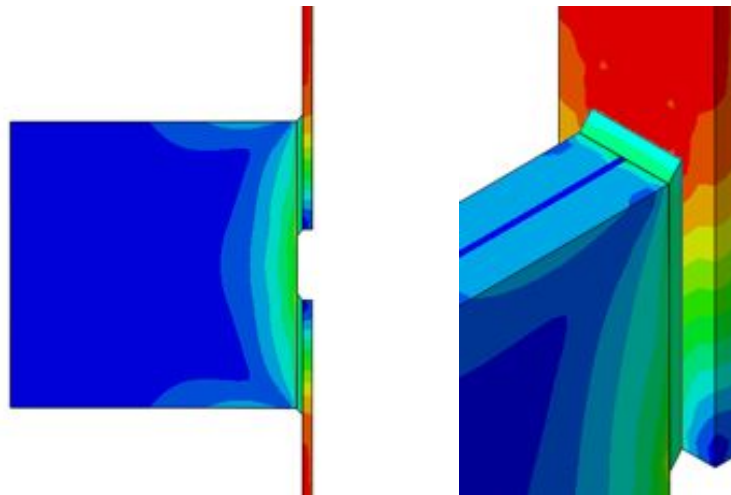


Figure 48 - FEM: deformed view (vertical scale x10)

6. Conclusions

The major conclusions are:

1. More experimental tests will have to be made in order to achieve a good characterization of the adhesive behaviour. A volumetric test or equivalent, able to evaluate without uncertainties the Poisson coefficient, is recommended.
2. Despite the uncertainties regarding the volumetric terms of the adhesive, the FEA on the uniaxial tension models showed that, with the material coefficients obtained through the fitting procedure of uniaxial test data, it is possible to simulate the corresponding tests with a reasonable agreement.
3. However, when the calibrated constitutive laws for uniaxial tension were applied on an adhesive layer subjected to shear and tension and also simple shear, the numerical output showed a very bad correlation with the test results. The reason to this could be the fact that the adhesive is now on a completely different and new type of stress state: shear. To overcome this problem, it is suggested the realization of future small-scale tests, like a planar test (pure shear). Having information about the shear behaviour of the adhesive, in addition to the uniaxial test data, a new calibration process will be able to accurately model the current hyperelastic material under multi-axial states of stress.

7. Outcomes

During the STSM, experimental and numerical results have been carefully analysed, interpreted and compared.

The work that has been done during the STSM will be continued and finalized in the weeks following the STSM.

The final aim is to collect all these comparisons in a common journal paper (partly drafted), which will be submitted to peer-reviewed journals, as well as in Conference papers. The researchers involved in this STSM feel confident that the STSM visit has contributed to a solid collaborative link between the two research institutions. In this context, the support of the COST Action TU1403 in facilitating this STSM is gratefully acknowledged.

8. References

- [1] Abaqus/CAE Benchmarks Manual – version 6.11 (2011). Dassault Systèmes Simulia Corp. USA.
- [2] Abaqus/CAE Theory Manual – version 6.11 (2011). Dassault Systèmes Simulia Corp. USA.
- [3] Abaqus/CAE User's Manual – version 6.11 (2011). Dassault Systèmes Simulia Corp. USA.
- [4] Abeln, B., Preckwinkel, E., Yandzio, E., Heywood, M., Netusil, M., Eliasova, M. and Grenier, C. (2013). "Development of innovative steel-glass structures in respect to structural and architectural design (INNOGLAST)". Final Report, Research Fund for Coal and Steel, European Commission, Luxembourg.

- [5] Antunes, P. et al (2008). "Hyperelastic Modelling of Cork-Polyurethane Gel Composites: Non-linear FEA Implementation in 3D Foot Model". Material Science Forum, Vols. 587-588, pp 700-705.
- [6] Bortoli, D. and Wrubleski, E. (2011). "Hyperfit – curve fitting software for incompressible hyperelastic material models". 21st Brazilian Congress of Mechanical Engineering, Natal, RN, Brazil.
- [7] Firmo, F. (2015). "Experimental/FEM study of hybrid steel-glass beams". Master thesis, Civil Engineering Department, DEC-FCTUC, University of Coimbra (in Portuguese).
- [8] Froling, M. (2013). "Strength design methods for glass structures". PhD Thesis. Department of construction sciences, Lund University.
- [9] Hoss, L. and Marczak, R. (2009). "Hyperelastic constitutive models for incompressible elastomers and soft tissues: fitting and performance comparison." 20th International Congress of Mechanical Engineering, Gramado, RS, Brazil.
- [10] http://solidmechanics.org/Text/Chapter3_5/Chapter3_5.php
- [11] http://www.qucosa.de/fileadmin/data/qucosa/documents/5995/data/Analysis_of_Hyperelastic_Materials_with_MECHANICA.pdf
- [12] Jordão, S., Cruz, P., Valente, I., Carvalho, P., Santiago, A., Silva, L. (2010). S-GLASS: Structural performance and design rules of glass beams externally reinforced. Research project funded by the Portuguese Foundation for Sciences and Technology under contract grant PTDC/ECM/116609/2010.
- [13] Netušil, M. (2011). "Hybrid Steel-Glass Beams". PhD thesis, Department of Steel and Timber Structures, Faculty of Civil Engineering, Czech Technical University, Prague.
- [14] Netušil, M. and Eliasova, M. (2014). "Trends and requirements for adhesives with load bearing roles". Challenging Glass 4 & COST Action TU0905 Final Conference
- [15] Nhamoinesu, S. and Overend, M. (2012). "The Mechanical Performance of Adhesives for a Steel-Glass Composite Façade System". Challenging Glass 3 – Conference on Architectural and Structural Applications of Glass,
- [15] Sasso, M. et al (2008). "Characterization of hyperelastic rubber-like materials by biaxial and uniaxial stretching tests based on optical methods" Polymer testing, Elsevier.
- [16] Silvestru, V. and Englhardt, O. (2014). "Application study for hybrid adhesively bonded glass-steel façade elements". Challenging Glass 4 & COST Action TU0905 Final Conference
- [17] Test Methods for Determining Hyperelastic Properties of Flexible Adhesives, in [http://www.adhesivestoolkit.com/Data/NPLDocuments/P%20A%20J/Measurement%20Notes/CMMT\(MN\)054%20hyperelastic.pdf](http://www.adhesivestoolkit.com/Data/NPLDocuments/P%20A%20J/Measurement%20Notes/CMMT(MN)054%20hyperelastic.pdf)
- [18] Valarinho, L. et al (2014). "Experimental and numerical study on GFRP-glass adhesively bonded joints". Challenging Glass 4 & COST Action TU0905 Final Conference
- [19] Vlad, C. and Prisacaru, G. (2014). "FEM Simulation on Uniaxial Tension of Hyperelastic Elastomers". Applied Mechanics and Materials.
- [20] Weller, B. and Nicklisch, F. (2010). "Bonding of Glass - Latest Trends and Research". ASCE 2010 Congress.

Involved Researchers

Mr. Filipe Firmo (Visitor), Early Stage Researcher (ESR) and currently Ph.D. Candidate at University of Coimbra, Department of Civil Engineering (Portugal).

Dr. Chiara Bedon (Host), ESR, currently Assistant Professor at University of Trieste, Department of Engineering and Architecture (Italy) and MC member for the ongoing COST Action TU1403.